Journal of
Materials Chemistry C

PAPER

View Article Online
View Journal | View Issue

Cite this: *J. Mater. Chem. C*, 2019, 7, 6105

Novel benzodithiophene unit with an alkylthiobiphenyl side chain for constructing high-efficiency polymer solar cells†

Xiaoming Li,‡[ab] Gongyue Huang,‡[b] Huanxiang Jiang,[b] Shanlin Qiao, *[a] Xiao Kang,[ab] Weichao Chen*[c] and Renqiang Yang *[b]

Received 25th February 2019,
Accepted 18th April 2019

DOI: 10.1039/c9tc01082c

rsc.li/materials-c

A novel BDT monomer with an alkylthiobiphenyl side chain named 4,8-bis(4′-((2-hexyldecyl)thio)-[1,1′-biphenyl]-4-yl)benzo[1,2-*b*:4,5-*b*′]dithiophene (BDTBPS) was designed and synthesized. The polymer named PBDTBPS–BDD was synthesized with BDTBPS and benzo[1,2-*b*:4,5-*b*′]dithiophene-4,8-dione (BDD). Solar cells were studied by blending the polymer PBDTBPS–BDD with both fullerene and 3,9-bis(2-methylene-(3-(1,1-dicyanomethylene)-indanone))-5,5,11,11-tetrakis(4-hexylphenyl)-dithieno[2,3-*d*:2′,3′-*d*′]-*s*-indaceno[1,2-*b*:5,6-*b*′]dithiophene (ITIC). The optimized polymer solar cells showed a PCE of 8.40% and 9.76% for the $PC_{71}BM$-based and ITIC-based solar cells, respectively. This research indicates that the novel monomer is a promising unit for constructing high-efficiency polymer solar cells.

1. Introduction

Polymer solar cells (PSCs) have attracted significant attention in recent years owing to their unique advantages, like flexibility, low cost and large-scale production.[1–4] A breakthrough has been achieved for the improvement of the power conversion efficiency (PCE) in the past few years.[5–7] Recently, high PCEs have been achieved for PSCs by blending a donor material with a fullerene or a non-fullerene acceptor material.[8–13] The PCE was determined by three key parameters, which are open-circuit voltage (V_{oc}), short-circuit current density (J_{sc}) and fill factor (FF).[14,15] Therefore, to achieve a brilliant PCE, the key points that we should pay more attention to are broad absorption spectra for a larger J_{sc}, a deep highest occupied molecular orbital (HOMO) energy level for a higher V_{oc} with a suitable lowest unoccupied molecular orbital (LUMO) energy level for efficient charge separation, and high hole mobility for a larger J_{sc} and FF.

Fullerenes and their derivatives, as the dominant acceptor materials, have been widely studied because of their high electron mobility, high electron affinity and isotropic charge transport.[16] Compared with fullerene acceptors, a classical non-fullerene acceptor material named 3,9-bis(2-methylene-(3-(1,1-dicyanomethylene)-indanone))-5,5,11,11-tetrakis(4-hexylphenyl)-dithieno-[2,3-*d*:2′,3′-*d*′]-*s*-indaceno[1,2-*b*:5,6-*b*′]dithiophene (ITIC) has been widely studied by many groups all over the world since it was reported by Zhan's group in 2015.[17–23] It is known that ITIC-based devices usually show higher V_{oc} than fullerene-based devices because of its relatively high LUMO energy level. On the other hand, ITIC-based devices show larger J_{sc} owing to the strong absorption in the near-infrared region, which generates wider absorption spectra when blended with appropriate donor materials. Recently, some novel donor materials blended with ITIC showed excellent photovoltaic performance; in particular, a few donor materials like PBDTS-NQx, J_{71} and PBDB-T have made the 11% PCE breakthrough for single-junction PSCs, which provides great inspiration and enlightenment for researchers.[8,22,24] Therefore, to realize commercial applications, designing novel high-efficiency donor materials is still imperative and full of challenges.

Benzo[1,2-*b*:4,5-*b*′]dithiophene (BDT) has been widely studied for constructing excellent donor materials in recent years.[2,25–29] Therein, side chain engineering is regarded as a valuable strategy to tune energy levels and absorption spectra of polymers. Recently, a novel BDT unit with an alkoxybiphenyl side chain was reported by our group.[30] The polymer-based alkoxybiphenyl-substituted BDT demonstrated a great J_{sc} because of its extended p-conjugation and good symmetry. Nevertheless, the V_{oc} was not prominent so the performance could not be further promoted. As we all know, the sulfur atom always shows unique characters in PSCs because of both its

[a] College of Chemistry and Pharmaceutical Engineering, Hebei University of Science and Technology, Shijiazhuang 050018, China. E-mail: qiaosl@qibebt.ac.cn
[b] Qingdao Institute of Bioenergy and Bioprocess Technology, Chinese Academy of Sciences, 189 Songling Road, Qingdao 266101, China. E-mail: yangrq@qibebt.ac.cn
[c] College of Textiles & Clothing, Qingdao University, Qingdao 266071, China. E-mail: chenwc@qdu.edu.cn

† Electronic supplementary information (ESI) available. See DOI: 10.1039/c9tc01082c

‡ These authors contributed equally to this work.

electron-donating ability and some p-acceptor capability.[22,31–35] Therefore, polymers with alkylthio side chains usually show a slightly broadened absorption spectrum and a lower HOMO energy level, which is beneficial for larger J_{sc} and higher V_{oc}. Therefore, the BDT monomer linking with the alkylthiobiphenyl group may be a good electron-donating unit for constructing high-performance polymer donor materials with both high V_{oc} and large J_{sc}.

Here, a novel monomer BDTBPS was synthesized by introducing an alkylthiobiphenyl side chain into the BDT core. The polymer PBDTBPS–BDD was obtained by the Stille coupling reaction using BDTBPS and benzo[1,2-*b*:4,5-*b*′]dithiophene-4,8-dione (BDD). The resulting polymer PBDTBPS–BDD exhibited high thermal stability. Moreover, the polymer showed a deep HOMO energy level of —5.30 eV. The photovoltaic performance was investigated by blending with both $PC_{71}BM$ and ITIC. Benefiting from the low HOMO, the optimized PSCs showed PCEs of 8.40% and 9.76% with high V_{oc} of 0.88 V and 0.96 V for $PC_{71}BM$-based and ITIC-based solar cells, respectively. This work demonstrated that the alkylthiobiphenyl side chain could improve the photovoltaic performance with an obvious effect.

2. Experimental section

2.1 Materials and reagents

Benzo[1,2-*b*:4,5-*b*′]dithiophene-4,8-dione was purchased from Derthon Optoelectronic Materials Sci. Tech. Co., Ltd; 1,3-bis-(5-bromothiophen-2-yl)-5,7-bis(2-ethylhexyl)-4*H*,8*H*-benzo[1,2-*c*:4,5-*c*′]dithiophene-4,8-dione (BDD-Br) was purchased from Solarmer Materials Inc. All of the chemicals were used as received. Tetrahydrofuran and toluene were dried over Na/benzophenone and freshly distilled prior to use. Other chemicals were commercial and were used as received. The general synthetic routes for the compound BDTBPS and its polymer PBDTBPS–BDD are shown in Scheme 1. The detailed synthetic routes are as follows.

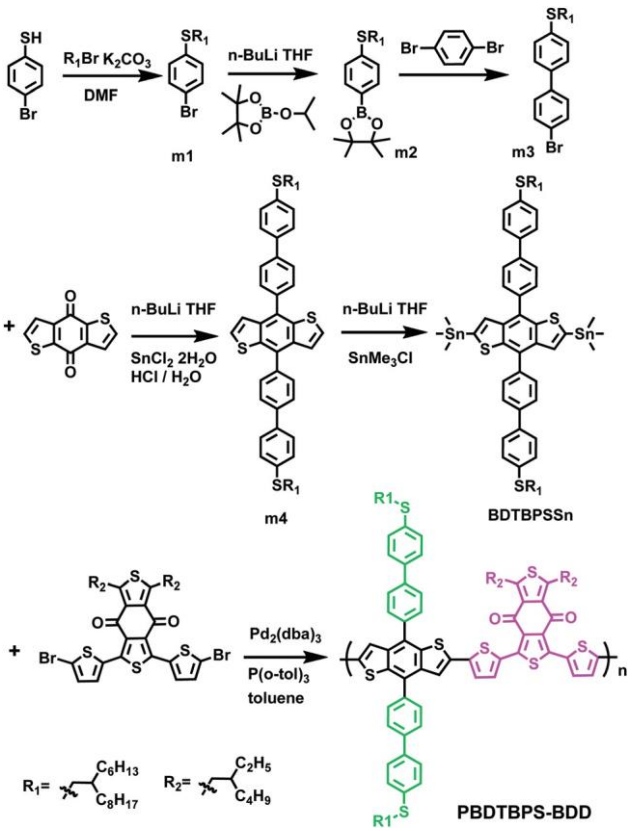

Scheme 1 The general synthetic routes for the compound BDTBPSSn and its polymer PBDTBPS–BDD.

Synthesis of compound m1

A mixture of 4-bromobenzenethiol (10 g, 52.9 mmol), 7-(bromomethyl)pentadecane (17.8 g, 58.2 mmol), potassium carbonate (14.6 g, 105.8 mmol) and *N*,*N*-dimethylformamide (DMF) (120 mL) was refluxed for 24 hours. The reaction mixture was extracted with dichloromethane (DCM), washed with water and dried with Na_2SO_4. After removing the solvent, the residue was purified by silica gel column chromatography with petroleum ether (PE) as the eluent solution to obtain 18.0 g of m1 as a colourless liquid with 82.2% yield. ^{1}H NMR (600 MHz, $CDCl_3$) d 7.40–7.35 (m, 2H), 7.18 (dd, *J* = 6.4, 4.7 Hz, 2H), 2.86 (d, *J* = 6.3 Hz, 2H), 1.63–1.58 (m, 1H), 1.44–1.34 (m, 4H), 1.30–1.21 (m, 21H), 0.88 (t, *J* = 6.7 Hz, 6H).

Synthesis of compound m2

A dried three-neck flask was charged with compound m1 (4.6 g, 11.12 mmol) and dry tetrahydrofuran (THF) (40 mL) under an argon atmosphere. *n*-BuLi (1.6 M, 9.0 mL) was slowly added to the solution at —78 1C and the mixture was stirred for 2 hours. Then the isopropoxyboronic acid pinacol ester (3.4 mL) was added dropwise at —78 1C and the mixture was stirred overnight at room temperature. The reaction was quenched by water and neutralized with diluted hydrochloric acid (HCl) until the pH was 7.0. Then the mixture was extracted with DCM and washed with water. After removing the solvent, the residue was purified by silica gel column chromatography with PE and DCM as the eluent solution to obtain 4.5 g of m2 as a colourless liquid with 87.9% yield. ^{1}H NMR (600 MHz, $CDCl_3$) d 7.68 (d, *J* = 8.0 Hz, 2H), 7.27 (d, *J* = 8.9 Hz, 4H), 2.91 (d, *J* = 6.3 Hz, 2H), 1.67–1.61 (m, 1H), 1.44–1.22 (m, 44H), 0.89–0.86 (m, 6H), —0.00 (s, 1H).

Synthesis of compound m3

A mixture of compound m2 (4.5 g, 9.77 mmol), 1,4-dibromobenzene (2.54 g, 10.75 mmol), $Pd(PPh_3)_4$ (0.45 g, 0.39 mmol), K_2CO_3 (6.8 g, 48.85 mmol), H_2O (10 mL), THF (10 mL) and toluene (40 mL) was refluxed overnight under an argon atmosphere. The reaction mixture was extracted with DCM and washed with water and then dried with Na_2SO_4. After removing the solvent, the residue was purified by silica gel column chromatography with PE and DCM as the eluent solution to obtain 2.5 g of m3 as a colourless liquid with 52.3% yield. ^{1}H NMR (600 MHz, $CDCl_3$) d 7.56–7.53 (m, 2H), 7.47–7.44 (m, 2H), 7.44–7.41 (m, 2H), 7.39–7.35 (m, 2H), 2.93 (d, *J* = 6.3 Hz, 2H), 1.69–1.60 (m, 1H), 1.40

(d, J = 21.1, 14.0, 8.0 Hz, 5H), 1.33–1.18 (m, 20H), 0.88 (t, J = 6.9 Hz, 6H).

Synthesis of compound m4

Compound m3 (8.5 g, 17.36 mmol) dissolved in THF (100 mL) was cooled to −78 °C under the protection of nitrogen. *n*-BuLi (8.7 mL, 20.83 mmol, 2.4 M) was dropped slowly into the solution. After keeping the mixture at −78 °C for 2 hours, benzo[1,2-*b*:4,5-*b*]dithiophen-4,8-dione (1.59 g, 7.23 mmol) was poured into the flask quickly. The mixture was stirred overnight at room temperature. $SnCl_2{\cdot}2H_2O$ dissolved in 10% HCl (50 mL) was injected and stirred for another 12 hours. The mixture was extracted by DCM and washed with water. 3.1 g of white solid (42.5% yield) was obtained after further purification by silica gel column chromatography. ^{1}H NMR (600 MHz, $CDCl_3$) δ 7.83–7.76 (m, 8H), 7.64 (d, J = 8.3 Hz, 4H), 7.44 (dd, J = 6.9, 3.7 Hz, 6H), 7.41 (d, J = 5.6 Hz, 2H), 2.98 (d, J = 6.2 Hz, 4H), 1.74–1.63 (m, 2H), 1.43 (ddt, J = 20.7, 13.6, 6.6 Hz, 8H), 1.35–1.24 (m, 40H), 0.89 (td, J = 6.8, 4.4 Hz, 12H). ^{13}C NMR (151 MHz, $CDCl_3$): 140.27, 138.19, 137.78, 137.36, 136.20, 130.12, 129.86, 129.04, 127.41, 127.20, 122.97, 77.23, 77.02, 76.80, 38.44, 37.59, 33.23, 31.90, 29.95, 29.61, 29.36, 26.55, 22.70, 14.13.

Synthesis of compound BDTBPSSn

n-BuLi (3.6 mL, 8.61 mmol, 2.4 M) was dropped slowly into a solution of compound m4 (3.1 g, 3.08 mmol) dissolved in dry THF (100 mL) under the protection of nitrogen at −78 °C. After keeping the mixture at −78 °C for 3 hours, trimethyltin chloride (10.8 mL, 10.78 mmol, 1.0 M) was injected into the flask quickly. The reaction was stirred overnight at room temperature and then stopped by the addition of water. The crude product was extracted by DCM and then the solution was removed. The crude product was purified by recrystallization from *n*-hexane. A faint yellow solid (3.38 g, 82.4% yield) was gained. ^{1}H NMR (600 MHz, $CDCl_3$) δ 7.82 (q, J = 8.3 Hz, 8H), 7.67 (d, J = 8.3 Hz, 4H), 7.48–7.41 (m, 6H), 2.98 (d, J = 6.2 Hz, 4H), 1.72–1.66 (m, 2H), 1.51–1.37 (m, 9H), 1.35–1.22 (m, 45H), 0.90 (dd, J = 6.8, 2.0 Hz, 12H), 0.52–0.19 (m, 18H). ^{13}C NMR (151 MHz, $CDCl_3$): 142.53, 142.25, 139.98, 138.89, 137.94, 137.20, 137.04, 130.65, 129.98, 129.10, 128.54, 127.43, 127.15, 77.24, 77.03, 76.82, 38.49, 37.62, 33.25, 31.92, 31.61, 29.96, 29.63, 29.37, 26.57, 22.70, 14.15, −8.31.

Synthesis of polymer PBDTBPS–BDD

Compounds BDTBPSSn (133.3 mg, 0.1 mmol), BDD–Br (76.7 mg, 0.1 mmol), $Pd_2(dba)_3$ (1.8 mg, 0.002 mmol), and P(*o*-tol)$_3$ (3.6 mg, 0.012 mmol) were added into a flask. The flask was subjected to three successive vacuum cycles followed by refilling with argon, and then 4 mL of dry toluene was added. The reaction mixture was heated to 110 °C carefully for 2 h under argon protection. The mixture was then cooled to room temperature and the polymer was precipitated by addition of methanol, then filtered and purified by Soxhlet extraction with methanol, chloroform, and *o*-dichlorobenzene (*o*-DCB) sequentially. The *o*-DCB solution was concentrated by evaporation and then precipitated into methanol. The purple solid was filtered to yield the desired polymer PBDTBPS–BDD (148 mg, 91.9% yield).

2.2 Fabrication and characterization of devices

Organic solar cells were tested with the conventional bulk heterojunction sandwich device structure of ITO/PEDOT:PSS/PBDTBPS–BDD:acceptor/PFN/Al. Patterned ITO-coated glass needed to be ultrasonically cleaned with ITO detergent, deionized water, acetone and isopropanol for 20 minutes each in the proper order. Subsequently, the substrates need to be exposed to the treatment of oxygen plasma for another 6 minutes. Next, PEDOT:PSS (Baytron PVP Al 4083) was spin-coated on the ITO-coated glass substrates before annealing at 160 °C for 30 minutes in a drying oven. Finally, the substrates were placed in a glove box. The blend solution of PBDTBPS–BDD and acceptor material ($PC_{71}BM$ or ITIC) in DCB was spin-coated onto the substrates, and PFN was spin-coated onto the active layer. Finally, the electrode Al (*ca.* 100 nm) was slowly deposited through a mask to define the active area of 0.10 cm^2 in a high vacuum degree of 10^{-5} orders of magnitude.

PCE was measured with a Keithley 2420 source measurement unit under the illumination of an AM 1.5G solar simulator with an intensity of 100 mW cm^{-2}. The EQE spectra for the PSCs were recorded using a certified Newport incident photon conversation efficiency (IPCE) measurement system.

The morphology of the blend films was determined by atomic force microscopy (AFM) and transmission electron microscopy (TEM) employing an Agilent 5400 with tapping mode and a JEOL JEM-1011 transmission electron microscope at an accelerating voltage of 100 kV, respectively.

3. Results and discussion

3.1 Synthesis and characterization

The general synthetic routes for the compound BDTBPSSn and polymer PBDTBPS–BDD are shown in Scheme 1. The chemical structures of the compounds were characterized by ^{1}H-NMR and ^{13}C-NMR spectra. The raw material 4-bromobenzenethiol reacted with bromoalkane to provide m1, which was used to prepare m2 by lithiation and reaction with isopropoxyboronic acid pinacol ester. The S-containing side chain of m3 was obtained by the Suzuki coupling reaction. The side chain was introduced into BDT *via* the normal procedure. Finally, the compound BDTBPSSn was obtained from the precursor BDTBPS by lithiation and then quenching with trimethyltin. Polymer PBDTBPS–BDD was synthesized by the Stille coupling reaction. The detailed synthesis was given in the Experiment section.

The number average molecular weight (M_n) of PBDTBPS–BDD was 21 kDa with a polydispersity index (PDI) of 2.3. The thermal properties of BDTBPS–BDD were measured by thermogravimetric analysis (TGA) in a nitrogen atmosphere at a heating rate of 10 °C min^{-1}. As shown in Fig. S1 (ESI†), PBDTBPS–BDD exhibited high thermal stability with an onset decomposition temperature (T_d) with 5% weight-loss located at *ca.* 394 °C.

3.2 Optical and electrochemical properties

The normalized optical ultraviolet-visible (UV-vis) absorption spectra of the polymer in *o*-DCB solution and as a solid film are shown in Fig. 1. Similar optical properties were found in solution and as a film. The PBDTBPS–BDD solution showed a main absorption peak at *ca.* 581 nm and a shoulder peak at *ca*. 623 nm. The film showed a main absorption peak at the same wavelength. As shown in Fig. 1a, the absorption spectrum was slightly red-shifted in film compared to in solution. Compared with the spectrum in *o*-DCB solution, the spectrum of film shows a similar absorption shape, which could be ascribed to the molecular aggregates in the solution.[26] The maximum absorption coefficients of PBDTBPS–BDD in *o*-DCB solution and solid film were measured, and the value for the solution was enhanced by *ca.* 78% compared with that of the film, as shown in Fig. 1b (0.91×10^5 *vs.* 0.51×10^5). The absorption onset (λ_{onset}) of PBDTBPS–BDD was 678 nm and the corresponding optical band gap was about 1.83 eV.

Cyclic voltammetry (CV) was employed to evaluate the electrochemical properties of PBDTBPS–BDD. As shown in Fig. S2 (ESI†), the HOMO energy level was calculated to be —5.30 eV from the onset oxidation potential (E_{ox}) of 0.96 eV. The corresponding LUMO energy level was about —3.47 eV, which was obtained from the difference between the HOMO energy level and the optical band gap. The deep HOMO energy level was conducive to realizing the high V_{oc} for the PSCs.

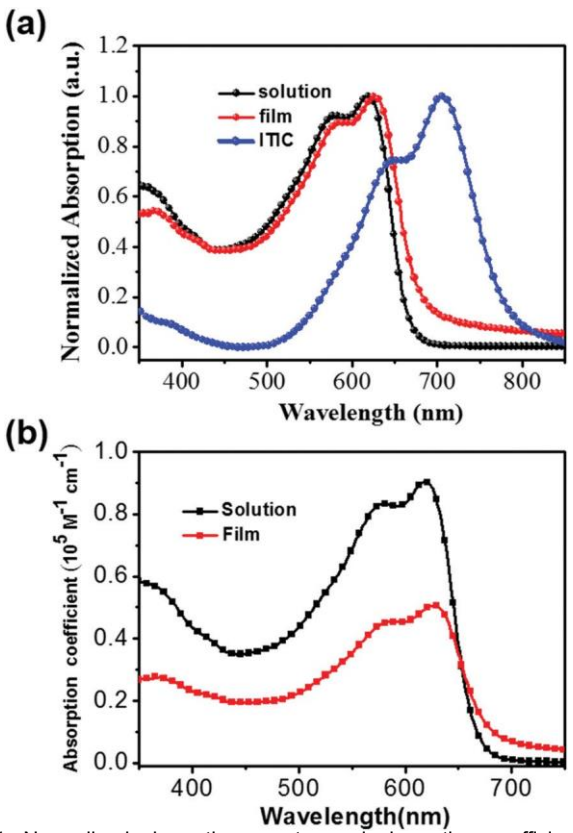

Fig. 1 Normalized absorption spectra and absorption coefficient of PBDTBPS–BDD in solution and as a solid film and an ITIC film.

3.3 Photovoltaic performance

BHJ solar cells based on $PC_{71}BM$ and ITIC as the acceptor were fabricated to investigate the photovoltaic properties of PBDTBPS–BDD. The devices with a conventional structure of glass/ITO/PEDOT:PSS/PBDTBPS–BDD:acceptor/PFN/Al had optimal ratios of 1 : 1.5 and 1 : 1 for $PC_{71}BM$ and ITIC, respectively. The corresponding PCEs of 6.81% and 7.33% were obtained for the $PC_{71}BM$-based solar cells and ITIC-based solar cells without any pretreatment, respectively. The device performance was improved after thermal annealing and the *J–V* curves are shown in Fig. S4 (ESI†) with different annealing temperatures. Furthermore, we investigated the effects of additives on the photovoltaic performance of the devices, but the performance was inferior to that of the thermally annealed devices as shown in Table S1 and Fig. S5 (ESI†).

For the $PC_{71}BM$-based solar cells, the PCE was increased to 8.40% owing to the enhanced J_{sc} after thermal annealing at 100 °C for 10 min. For ITIC-based solar cells, the optimal PCE of 9.76% was achieved, which benefited from the obvious enhanced J_{sc} and FF after thermal annealing at 100 °C for 10 min. The typical *J–V* curves of the optimal devices are shown in Fig. 2a. The corresponding photovoltaic parameters are summarized in Table 1. The ITIC-based solar cells showed a higher V_{oc} (0.96 V *vs.* 0.88 V) and a larger J_{sc} (17.17 mA cm^{-2} *vs.* 14.02 mA cm^{-2}) than the $PC_{71}BM$-based solar cells, which was derived from the higher LUMO energy level and wider absorption spectrum of ITIC than $PC_{71}BM$. The typical EQE curves of the optimal devices based on $PC_{71}BM$ and ITIC are shown in Fig. 2b. The two devices showed high EQE values with a peak near 80%. Compared with the $PC_{71}BM$-based solar cells, the solar cells based on ITIC exhibited a broader photoresponse range from 300 to 800 nm, which profited from the strong absorption of ITIC in the near-infrared region and therefore the good spectral complementarity between PBDTBPS–BDD and ITIC. The integrated current densities (J_{sc}^{EQE}) from the EQE spectra are 13.54 and 16.76 mA cm^{-2} for the $PC_{71}BM$- and ITIC-based devices, respectively, consistent with the J_{sc} values measured from the solar cell devices with a small deviation of around 5%. Therefore, the ITIC-based device showed larger J_{sc} than the $PC_{71}BM$-based device.

The photoluminescence (PL) spectra of the pure polymer and blend films were measured to investigate the photo-induced electron transfer behavior between the polymer and the $PC_{71}BM$ or ITIC. As shown in Fig. 3a, these blends of polymer:ITIC ($PC_{71}BM$) demonstrated a high proportion of quenching in comparison with the PL spectrum of the pure polymer. High PL quenching efficiency means that these devices have an effective charge transfer and exciton separation, which are in agreement with the higher J_{sc} values of the related devices. In addition, the relationship between the photocurrent (J_{ph}) and the effective applied voltage (V_{eff}) was studied to further analyze the charge generation, transport and extraction for the PBDTBPS–BDD-based devices (Fig. 3b).

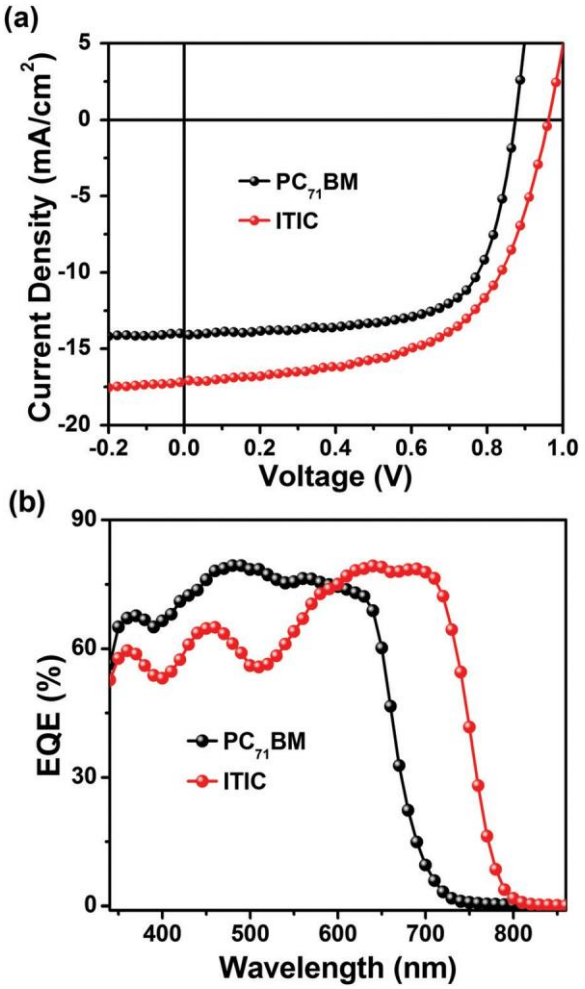

Fig. 2 (a) The *J*–*V* curves and (b) EQE curves of the optimal devices based on $PC_{71}BM$ and ITIC, respectively.

Table 1 Photovoltaic parameters of the optimal solar cells based on $PC_{71}BM$ and ITIC

Acceptor	V_{oc} (V)	J_{sc} (mA cm^{-2})	FF (%)	PCE[a] (PCE$_{max}$) (%)
$PC_{71}BM$	0.88 ± 0.01	11.48 ± 0.20	66.47 ± 0.10	6.71 ± 0.12 (6.81)
$PC_{71}BM$[b]	0.88 ± 0.01	13.86 ± 0.18	68.81 ± 0.08	8.29 ± 0.11 (8.40)
ITIC	0.95 ± 0.01	14.87 ± 0.15	51.34 ± 0.11	7.24 ± 0.14 (7.33)
ITIC[b]	0.94 ± 0.02	17.01 ± 0.16	59.12 ± 0.07	9.65 ± 0.11 (9.76)

[a] Standard deviations are obtained from 20 devices. [b] With 100 °C thermal annealing.

$J_{ph} = J_L - J_D$, where J_D and J_L represent the current density in the dark and under illumination, respectively. The effective voltage is $V_{eff} = V_0 - V_{appl}$, where V_0 is the voltage when $J_{ph} = 0$, and V_{appl} stands for the applied voltage. For the optimized device, the charge dissociation probabilities, P_{diss} (J_{ph}/J_{sat}, where J_{sat} is the saturated current density), for PBDTBPS–BDD:ITIC and PBDTBPS–BDD:PCBM are calculated to be 89.8% and 95.3%, respectively, which suggests that the PBDTBPS–BDD:PCBM has some advantages in improving charge extraction and suppressing molecule recombination, but owing to the limitation of the

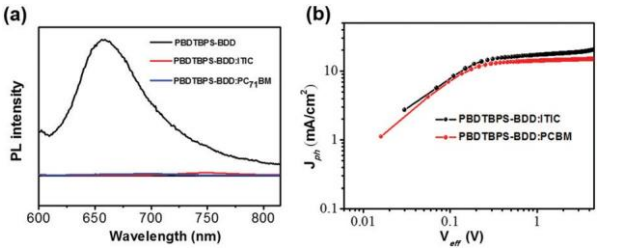

Fig. 3 (a) PL spectra of the polymer and the related blend films. (b) The curves of the photocurrent density (J_{ph}) *vs.* the effective bias (V_{eff}) for the two blend films.

absorption region, the J_{sc} was lower compared with that for ITIC.

3.4 Morphology of the blend films

The morphologies of the blend films were investigated by AFM and TEM. As shown in Fig. 4a and b, the polymer presented a good film-forming property when blended with $PC_{71}BM$ and ITIC. The blend films exhibited a smooth surface morphology with a root mean square (RMS) surface roughness of *ca.* 1.49 nm and 1.78 nm for blending with $PC_{71}BM$ and ITIC, respectively. However, the blends presented different bulk morphologies, as shown in Fig. 4c and d. An obvious nanofibrillar structure was observed in the PBDTBPS–BDD:$PC_{71}BM$ blends, which was not found in the PBDTBPS–BDD:ITIC blends. As a comparison, the PBDTBPS–BDD:ITIC blends exhibited a finely dispersed phase separation without the polymer fibres, which is similar to the other non-fullerene systems.[36] The appearance of the nanofibrillar structure may have constructed the good interpenetrating network in the PBDTBPS–BDD:$PC_{71}BM$ blends, which favours exciton dissociation and charge transport and therefore improved the FF in the $PC_{71}BM$-based solar cells.

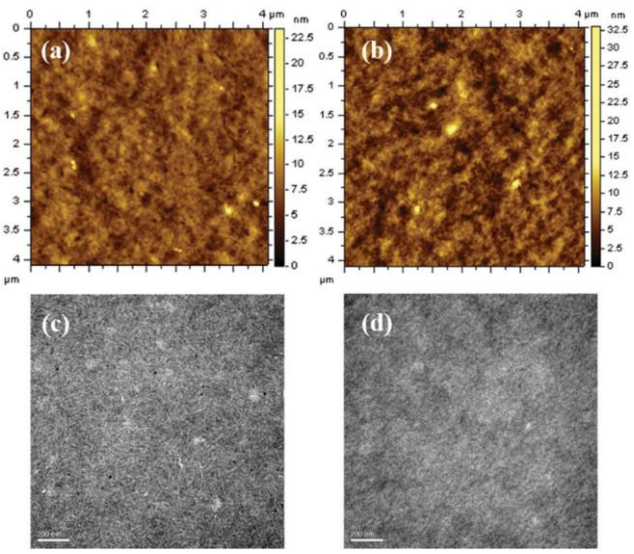

Fig. 4 (a) AFM height image and (c) TEM image of optimal PBDTBPS–BDD:$PC_{71}BM$ blend film. (b) AFM height image and (d) TEM image of optimal PBDTBPS–BDD:ITIC blend film.

Table 2 The charge carrier mobilities of the optimal blend films

Device	μ_e ($cm^2 V^{-1} s^{-1}$)	μ_h ($cm^2 V^{-1} s^{-1}$)	μ_h/μ_e
PBDTBPS–BDD:$PC_{71}BM$	5.93×10^{-4}	5.25×10^{-4}	0.89
PBDTBPS–BDD:ITIC	1.02×10^{-4}	1.45×10^{-4}	1.42

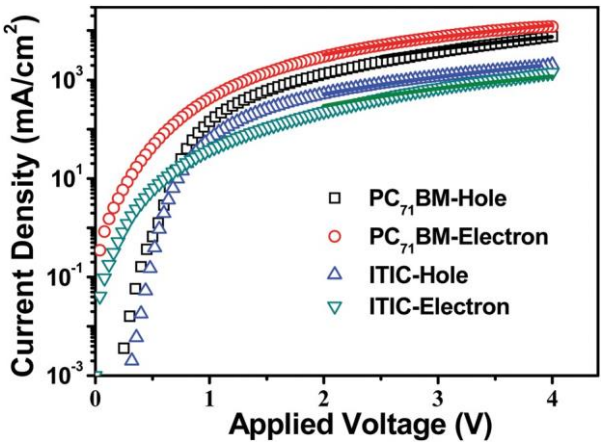

Fig. 5 *J–V* curves of vertical diodes with the device structures of ITO/PEDOT:PBDTBPS–BDD:acceptor/Au for hole only devices, and ITO/ZnO/PBDTBPS–BDD:acceptor/PFN/Al for electron only devices.

3.5 Charge carrier mobility of the blend films

The transport characteristics were investigated using the space charge-limited-current model to measure hole and electron mobilities in the blend films with the device structures of ITO/PEDOT:PBDTBPS–BDD:acceptor/Au and ITO/ZnO/PBDTBPS–BDD:acceptor/PFN/Al. As shown in Table 2, a hole mobility of 5.25×10^{-4} cm^2 V^{-1} s^{-1} and an electron mobility of 5.93×10^{-4} $cm^2 V^{-1} s^{-1}$ were obtained for the $PC_{71}BM$-based film and a hole mobility of 1.45×10^{-4} $cm^2 V^{-1} s^{-1}$ and an electron mobility of 1.02×10^{-4} $cm^2 V^{-1} s^{-1}$ were obtained for the ITIC-based film (the corresponding film thicknesses are shown in Table S2, ESI†). Meanwhile, hole to electron mobility ratios (μ_h/μ_e) of 0.89 and 1.42 were obtained for the $PC_{71}BM$-based and ITIC-based films, respectively. Consequently, the larger mobilities and more balanced charge carrier transport of the $PC_{71}BM$-based blend film contributed to achieving the higher FF (Fig. 5).[36]

4. Conclusion

In conclusion, a novel BDT unit with an alkylthiobiphenyl side chain named BDTBPS was designed and synthesized. The corresponding polymer PBDTBPS–BDD was designed and synthesized. The optimized PSCs showed PCE of 8.40% and 9.76% for the $PC_{71}BM$-based and ITIC-based films, respectively. This research indicated that the novel monomer is a promising monomer for constructing high-efficiency PSCs.

Conflicts of interest

There are no conflicts to declare.

Acknowledgements

This work was supported by the National Natural Science Foundation of China (51773220, 21805068, 51573205, 21502205 and 61405209), the Shandong Provincial Natural Science Foundation (ZR2017ZB0314), and DICP & QIBEBT (DICP&QIBEBT UN201709), Dalian National Laboratory for Clean Energy (DNL) CAS.

Notes and references

1 L. Lu, T. Zheng, Q. Wu, A. M. Schneider, D. Zhao and L. Yu, *Chem. Rev.*, 2015, 115, 12666–12731.
2 H. Yao, L. Ye, H. Zhang, S. Li, S. Zhang and J. Hou, *Chem. Rev.*, 2016, 116, 7397–7457.
3 L. Dou, Y. Liu, Z. Hong, G. Li and Y. Yang, *Chem. Rev.*, 2015, 115, 12633–12665.
4 Y. Li, *Acc. Chem. Res.*, 2012, 45, 723–733.
5 M. Li, K. Gao, X. Wan, Q. Zhang, B. Kan, R. Xia, F. Liu, X. Yang, H. Feng, W. Ni, Y. Wang, J. Peng, H. Zhang, Z. Liang, H.-L. Yip, X. Peng, Y. Cao and Y. Chen, *Nat. Photonics*, 2017, 11, 85–90.
6 F. Zhao, S. Dai, Y. Wu, Q. Zhang, J. Wang, L. Jiang, Q. Ling, Z. Wei, W. Ma, W. You, C. Wang and X. Zhan, *Adv. Mater.*, 2017, 29, 1700144.
7 J. Yuan, Y. Zhang, L. Zhou, G. Zhang, H.-L. Yip, T.-K. Lau, X. Lu, C. Zhu, H. Peng, P. A. Johnson, M. Leclerc, Y. Cao, J. Ulanski, Y. Li and Y. Zou, *Joule*, 2019, 3, 1–12.
8 X. Li, G. Huang, N. Zheng, Y. Li, X. Kang, S. Qiao, H. Jiang, W. Chen and R. Yang, *Sol. RRL*, 2019, 1900005, DOI: 10.1002/solr.201900005.
9 H. Li, D. He, P. Mao, Y. Wei, L. Ding and J. Wang, *Adv. Energy Mater.*, 2017, 7, 1602663.
10 F. Lin, W. Huang, H. Sun, J. Xin, H. Zeng, T. Yang, M. Li, X. Zhang, W. Ma and Y. Liang, *Chem. Mater.*, 2017, 29, 5636–5645.
11 D. Zhu, X. Bao, Q. Zhu, C. Gu, M. Qiu, S. Wen, J. Wang, B. Shahid and R. Yang, *Energy Environ. Sci.*, 2017, 10, 614–620.
12 J. Li, Y. Wang, Z. Liang, N. Wang, J. Tong, C. Yang, X. Bao and Y. Xia, *ACS Appl. Mater. Interfaces*, 2019, 11, 7022–7029.
13 W. Chen, M. Xiao, L. Han, J. Zhang, H. Jiang, C. Gu, W. Shen and R. Yang, *ACS Appl. Mater. Interfaces*, 2016, 8, 19665–19671.
14 Y.-J. Cheng, S.-H. Yang and C.-S. Hsu, *Chem. Rev.*, 2009, 109, 5868–5923.
15 D. Veldman, S. C. J. Meskers and R. A. J. Janssen, *Adv. Funct. Mater.*, 2009, 19, 1939–1948.
16 Y. He and Y. Li, *Phys. Chem. Chem. Phys.*, 2011, 13, 1970–1983.
17 Y. Lin, J. Wang, Z.-G. Zhang, H. Bai, Y. Li, D. Zhu and X. Zhan, *Adv. Mater.*, 2015, 27, 1170–1174.
18 L. Gao, Z. G. Zhang, H. Bin, L. Xue, Y. Yang, C. Wang, F. Liu, T. P. Russell and Y. Li, *Adv. Mater.*, 2016, 28, 8288–8295.
19 G. E. Park, S. Choi, S. Y. Park, D. H. Lee, M. J. Cho and D. H. Choi, *Adv. Energy Mater.*, 2017, 7, 1700566.

20 Z. Li, K. Jiang, G. Yang, J. Y. L. Lai, T. Ma, J. Zhao, W. Ma and H. Yan, *Nat. Commun.*, 2016, 7, 13094.
21 W. Zhao, S. Zhang and J. Hou, *Sci. China: Chem.*, 2016, 59, 1574–1582.
22 T. Yu, X. Xu, G. Zhang, J. Wan, Y. Li and Q. Peng, *Adv. Funct. Mater.*, 2017, 27, 1701491.
23 B. Fan, K. Zhang, X. F. Jiang, L. Ying, F. Huang and Y. Cao, *Adv. Mater.*, 2017, 29, 1606396.
24 W. Zhao, D. Qian, S. Zhang, S. Li, O. Inganas, F. Gao and J. Hou, *Adv. Mater.*, 2016, 28, 4734–4739.
25 W. Chen, G. Huang, X. Li, H. Wang, Y. Li, H. Jiang, N. Zheng and R. Yang, *ACS Appl. Mater. Interfaces*, 2018, 10, 42747–42755.
26 W. Chen, Z. Du, L. Han, M. Xiao, W. Shen, T. Wang, Y. Zhou and R. Yang, *J. Mater. Chem. A*, 2015, 3, 3130–3135.
27 W. Chen, H. Jiang, G. Huang, J. Zhang, M. Cai, X. Wan and R. Yang, *Sol. RRL*, 2018, 2, 1800101.
28 X. Gong, G. Li, C. Li, J. Zhang and Z. Bo, *J. Mater. Chem. A*, 2015, 3, 20195–20200.
29 K. Kranthiraja, K. Gunasekar, W. Cho, M. Song, Y. G. Park, J. Y. Lee, Y. Shin, I.-N. Kang, A. Kim, H. Kim, B. Kim and S.-H. Jin, *Macromolecules*, 2014, 47, 7060–7069.
30 D. Ding, W. Chen, J. Wang, M. Qiu, H. Zheng, J. Ren, M. Fan, M. Sun and R. Yang, *J. Mater. Chem. C*, 2016, 4, 8716–8723.
31 C. Cui, W.-Y. Wong and Y. Li, *Energy Environ. Sci.*, 2014, 7, 2276–2284.
32 H. Kim, B. Lim, H. Heo, G. Nam, H. Lee, J. Y. Lee, J. Lee and Y. Lee, *Chem. Mater.*, 2017, 29, 4301–4310.
33 B. Kan, Q. Zhang, F. Liu, X. Wan, Y. Wang, W. Ni, X. Yang, M. Zhang, H. Zhang, T. P. Russell and Y. Chen, *Chem. Mater.*, 2015, 27, 8414–8423.
34 B. Kan, Q. Zhang, M. Li, X. Wan, W. Ni, G. Long, Y. Wang, X. Yang, H. Feng and Y. Chen, *J. Am. Chem. Soc.*, 2014, 136, 15529–15532.
35 H. Jiang, X. Li, Z. Liang, G. Huang, W. Chen, N. Zheng and R. Yang, *J. Mater. Chem. A*, 2019, 7, 7760–7765.
36 J. Li, Z. Liang, Y. Wang, H. Li, J. Tong, X. Bao and Y. Xia, *J. Mater. Chem. C*, 2018, 6, 11015–11022.